Effect of crack width and wet-dry cycles on the chloride penetration resistance of engineered cementitious composite (ECC)

Sun, Renjuan; Lu, Wei; Tawfek, Abdullah M. ; Guan, Yanhua ; Hu, Xinlei ; Zhang, Hongzhi; Ling, Yifeng ; Šavija, Branko

DOI
10.1016/j.conbuildmat.2022.129030

Publication date
2022

Document Version
Final published version

Published in
Construction and Building Materials

Citation (APA)
Sun, R., Lu, W., Tawfek, A. M., Guan, Y., Hu, X., Zhang, H., Ling, Y., & Šavija, B. (2022). Effect of crack width and wet-dry cycles on the chloride penetration resistance of engineered cementitious composite (ECC). *Construction and Building Materials*, *352*, Article 129030. https://doi.org/10.1016/j.conbuildmat.2022.129030

Construction and Building Materials 352 (2022) 129030

Contents lists available at ScienceDirect

Construction and Building Materials

journal homepage: www.elsevier.com/locate/conbuildmat

Effect of crack width and wet-dry cycles on the chloride penetration resistance of engineered cementitious composite (ECC)

Renjuan Sun [a], Wei Lu [a], Chuanyi Ma [b], Abdullah M. Tawfek [a,c], Yanhua Guan [a], Xinlei Hu [a], Hongzhi Zhang [a,d,*], Yifeng Ling [a,*], Branko Šavija [e]

[a] School of Qilu Transportation, Shandong University, 250002 Jinan, PR China
[b] Shandong Hi-Speed Engineering Test CO., LTD, 250002 Jinan, PR China
[c] Sana'a University, 12544 Sanaa, Yemen
[d] Suzhou Research Institute, Shandong University, 215021 Suzhou, PR China
[e] Microlab, Faculty of Civil Engineering and Geosciences, Delft University of Technology, 2628 CN, Delft, the Netherlands

ARTICLE INFO

Keywords:
Engineered Cementitious Composites
Chloride penetration resistance
Crack width
Wet-dry cycles
Chloride binding isotherm
Microstructure

ABSTRACT

The resistance of cracked ECC against chloride ingress is mainly governed by the accumulated crack width of all the cracks rather than the maximum width of multiple cracks. However, most studies focus on the influence of a single fine crack (<100 μm), which is far smaller than the accumulated crack width. To this end, this study focuses on a relatively large crack width scale. Cracks with widths of 0.1, 0.2 and 0.3 mm were notched on an ECC specimen. Both NaCl solution immersion and wet-dry cycles conditions were applied. Chloride penetration profile as well as the change of total and water-soluble chloride ion content was measured. Relationship between the bound chloride and water-soluble chloride was studied. X-ray diffraction (XRD) and mercury intrusion porosimetry (MIP) tests were carried out to show the influence of crack width and wet-dry cycles on the changes of the mineral phases, porosity and pore size distribution in the vicinity of the crack.

1. Introduction

Chloride-induced corrosion of reinforcement is considered as one of the primary causes of deterioration of reinforced concrete structures, especially in the marine environment [1–3]. As the chloride can ingress into concrete by combined diffusion and absorption under unsaturated conditions, structures in tidal and splash zones are considered to be at most risk [4]. Therefore, considerable research has been conducted on understanding the influence of wet-dry cycles on the chloride penetration in concrete [5–7].

Concrete structures are prone to cracking under mechanical or environmental loads during their service life. The presence of cracks not only causes a loss of stiffness and bearing capacity of structural members, but also provides accessible channels for transport of moisture and chloride ions, thus accelerating the chloride ingress [8,9]. Crack width is one of the main factors affecting chloride transport in concrete [10,11]. It was found that the influence of crack width on chloride diffusion behaviors in concrete materials had lower and upper thresholds [12], with transport properties being essentially unaffected by cracking when the crack width is less than a certain threshold. Once the crack width is greater than the upper threshold, the ingress of chloride along the crack surface is consistent with that of the external (i.e. exposed) surface. Jang et al. [13] reported an upper threshold crack width of about 55 ~ 80 μm. Li et al. [14] reported the lower and upper threshold of 0.05 mm and 0.1 mm, respectively. Ismail et al. [15] showed that crack width<53 μm did not increase chloride diffusion. Wang et al. [16] reported the lower threshold and upper threshold were 0.05 mm and 0.2 mm respectively. Besides the crack width, other crack parameters also have an impact on chloride penetration, including the orientation [17], density [18], and roughness [19]. Differences in reported threshold crack widths can be attributed to those factors. For example, a load induced crack is more torturous than a notched one, which would give a large value of the threshold.

Engineered Cementitious Composite (ECC) is a strain-hardening cementitious material with a deformation capacity about two orders of magnitude larger than that of plain concrete under tension [20–22]. Previous investigations have shown that chloride diffusion coefficient of ECC was only about 1/2 that of mortar and 10 %–35 % that of concrete [23–25]. Reinforced ECC is therefore expected to have better durability compared with conventional reinforced concrete. Considering the high

* Corresponding authors at: School of Qilu Transportation, Shandong University, 250002 Jinan, PR China.
E-mail addresses: hzzhang@sdu.edu.cn (H. Zhang), yfling@sdu.edu.cn (Y. Ling).

https://doi.org/10.1016/j.conbuildmat.2022.129030
Received 27 April 2022; Received in revised form 18 August 2022; Accepted 30 August 2022
Available online 9 September 2022

Table 1
Chemical constituents of cementitious materials (wt.%).

Oxides	CaO	SiO_2	Al_2O_3	Fe_2O_3	MgO	SO_3	Na_2O	K_2O	TiO_2	MnO	P_2O_5
Cement	63.21	18.48	6.74	3.45	3.24	3.16	0.17	0.53	0.35	0.27	0.16
Fly ash	3.43	49.66	35.97	5.77	0.63	1.12	0.62	0.93	0.99	0.04	0.28

Table 2
Mix proportion of ECC (kg/m^3).

Cement	Fly ash	Sand	VMA	Water	Superplasticizer	Fiber
568	682	455	0.57	325	10	26

cost of ECC, it is generally used in parts of a structure under high static/fatigue stress and strain [26–32]. Multiple fine cracks are successfully generated on the ECC cover under load with enhanced deformation capacity of the hybrid ECC concrete system. Although it is generally believed that such fine cracks can effectively limit the penetration of chloride ions, studies have shown that the resistance of cracked ECC against chloride ingress is mainly governed by the accumulated crack width rather than the maximum one [33,34]. Therefore, influence of a relatively large crack width, typically>0.1 mm, on the chloride penetration should be reviewed.

Considering the difficulties on controlling the accumulated crack width of ECC, cracks with widths of 0.1 mm, 0.2 mm and 0.3 mm were notched on the ECC specimens herein. Both NaCl solution immersion and wet-dry cycles conditions were applied. Chloride penetration profile as well as the change of total and water-soluble chloride ion content was measured. Relationship between the bound chloride and water-soluble chloride was studied. X-ray diffraction (XRD) and mercury intrusion porosimetry (MIP) tests were carried out to show the influence of crack width and wet-dry cycles on the changes of the mineral phases, porosity and pore size distribution in the vicinity of the crack.

2. Materials and experimental program

2.1. Materials and proportions

The raw materials of ECC consisted of P.O. 42.5 Portland cement, Class F fly ash, local quartz sand with grain size ranging from 125 to 180 μm, polyvinyl-alcohol (PVA) fiber, Hypromellose-type viscosity modifying admixture (VMA) and polycarboxylic superplasticizer. The PVA fibers were produced by the Kuraray company, Japan. The chemical compositions of the used cement and fly ash as provided by the supplier are given in Table 1. A water to binder ratio (w/b) of 0.26 was used. The mix proportion of ECC used is shown in Table 2. As shown in the authors' previous study [35], the resulting ECC possesses a 28-day compressive strength and elastic modulus of 48.6 MPa and 21.5 GPa, respectively. The direct tensile strength and strain of this material are about 4.2 MPa and 4.2 %, respectively.

2.2. Specimens and exposure conditions

Prismatic specimens with size of 53 × 40 × 35 mm cured in a room with relative humidity of 95 % and temperature of 20 ± 2 °C for 28 days were used for the chloride penetration test. Cement, fly ash, quartz sand

Table 3
Test configurations.

Name	Exposure condition	Crack width (mm)
IM-CW0	Immersion	–
IM-CW1		0.1
IM-CW2		0.2
IM-CW3		0.3
WD-CW0	Wet-dry cycles	–
WD-CW1		0.1

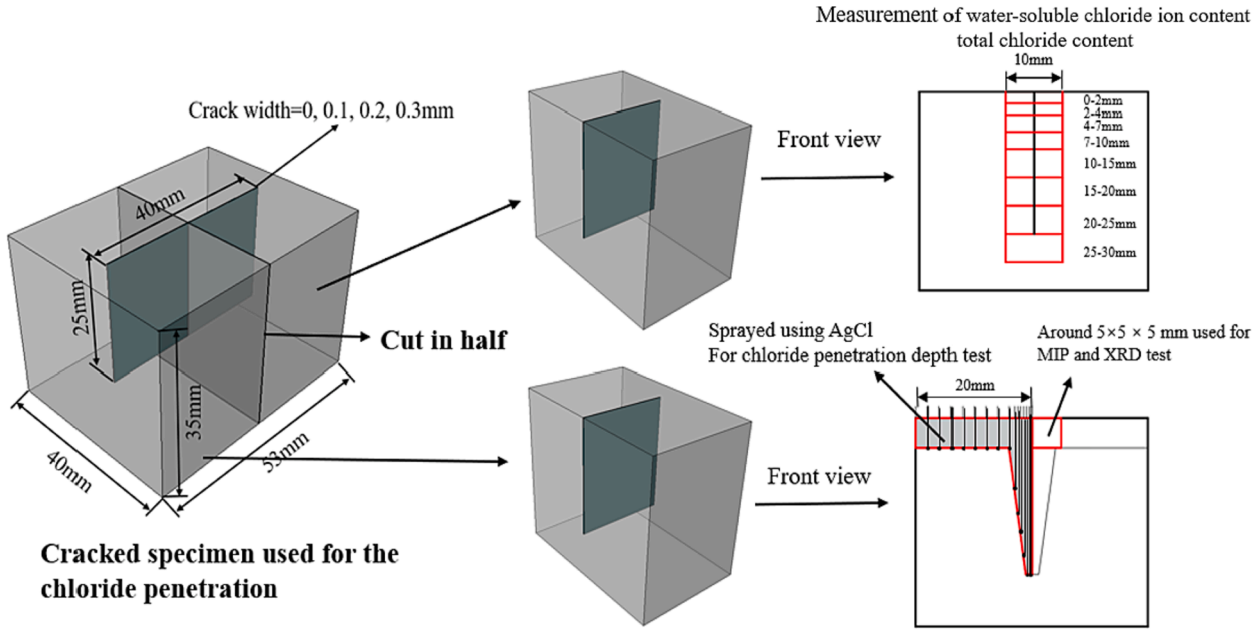

Fig. 1. Schematic view of the specimen used for the analysis.

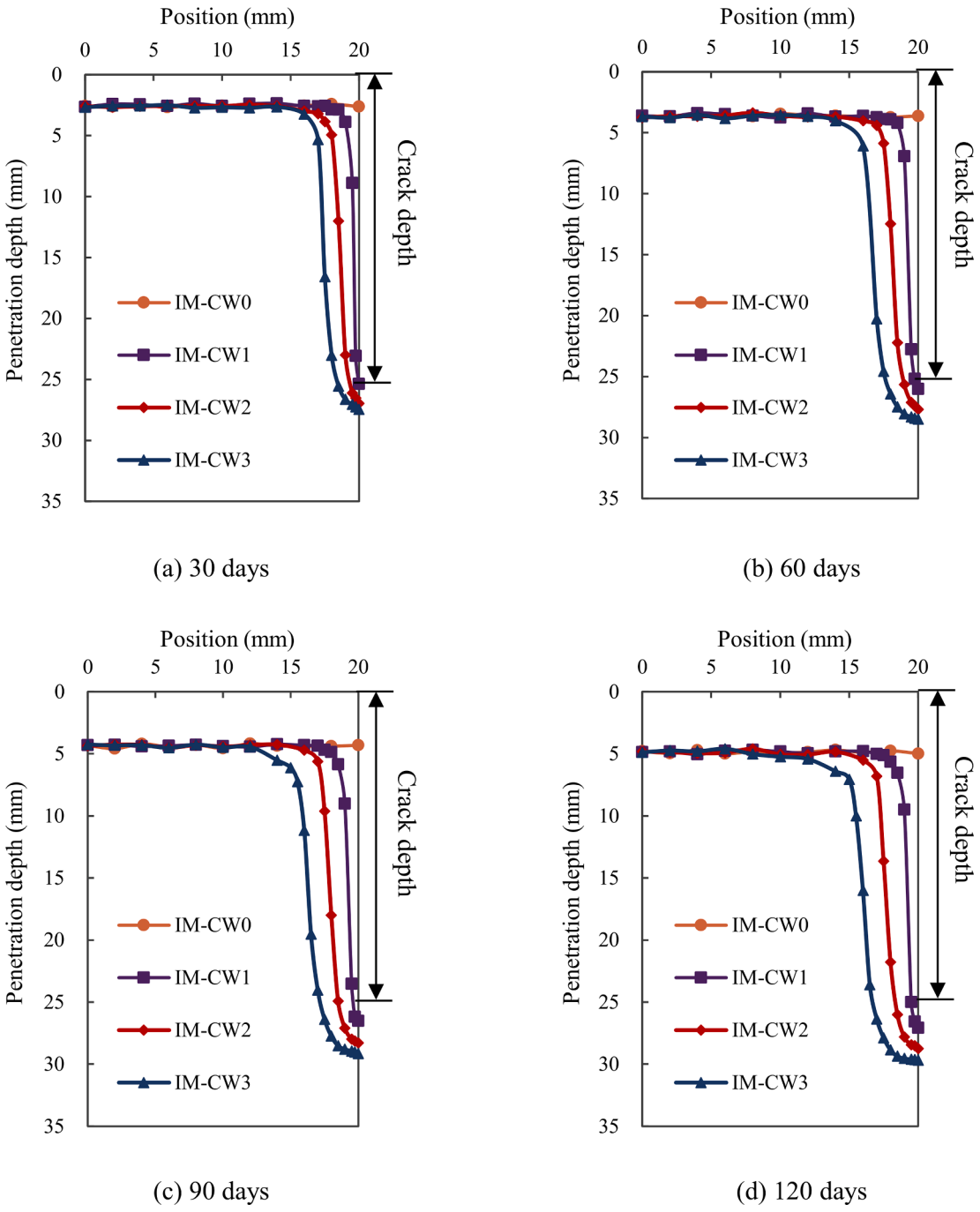

Fig. 2. Chloride penetration profile of specimens with different crack widths and diffusion duration.

and VMA were first mixed for two minutes. Water and superplasticizer were then added to the mixture and mixed under medium speed for 4 min. Afterwards, fibers were added with low mixing speed. This procedure was completed within one minute. The mixing was resumed for another 3 min mixing at medium speed. After mixing, the fresh mixture was poured into the molds. More details for the mixing process can be found in [35]. A crack was created on the middle line of surface with size of 53 × 40 mm, which is parallel to the long side, see Fig. 1. A steel sheet of certain thickness was used to create the cracks in the middle of specimen with a depth of about 25 mm. The generated crack widths are 0.1 mm, 0.2 mm and 0.3 mm, respectively. A specimen with no crack was produced as reference. The cracked surface was left open for the chloride penetration while the other sides were coated with epoxy resin. The same surface was used for the chloride penetration for the reference specimen. The specimens were then subjected to the exposure environment for chloride ingress. Afterwards, the specimen was cut as shown in Fig. 1 for the free chloride content, chloride penetration depth, X-ray diffractometer (XRD) and mercury intrusion porosimetry (MIP)

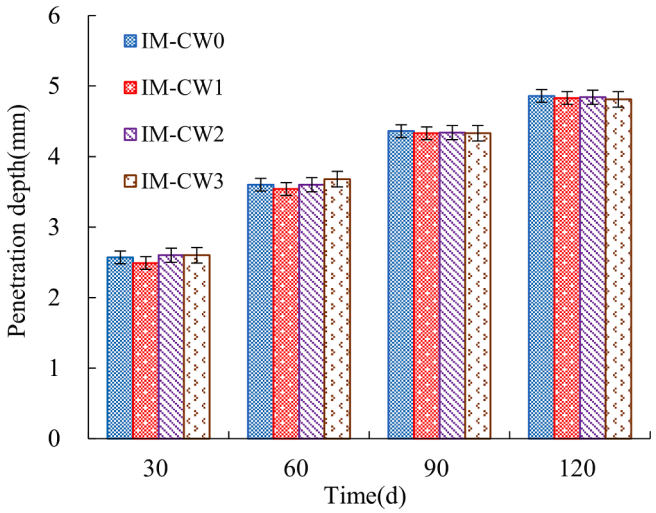

Fig. 3. Variations of chloride penetration depth with time at the position far away (i.e. 12 mm) from the crack.

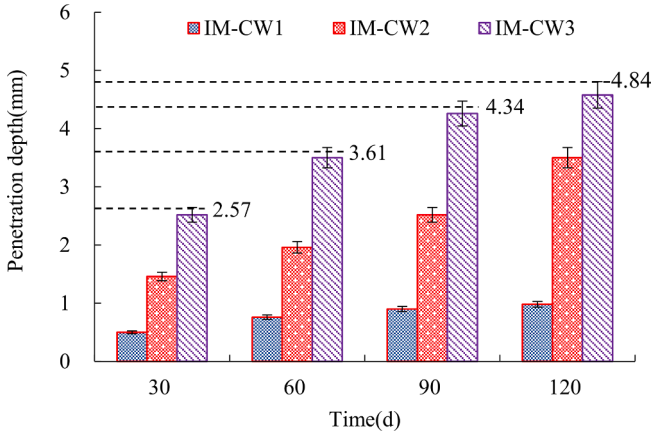

Fig. 4. Chloride penetration depths perpendicular to the crack wall at crack depth of 10 mm (The dash lines correspond to the chloride penetration depth of sounded area at various exposure periods).

measurements.

Two exposure conditions were considered. The first was soaking specimens in the 3.5 wt% NaCl solution. The temperature was kept at 20 ± 2 °C The second was wet-dry cyclic condition. The dry-wet cycle scheme was as follows: the specimen was soaked in the NaCl solution for 3 days and then oven dried at 60 °C [36] for the other 3 days. After a certain period, the specimens were taken out for analysis. Table 3 summarizes the conditions of all the cases. For each case, four exposure periods were considered: 30, 60, 90, and 120d. Three specimens were tested for each case under a certain exposure time. The average value was used.

2.3. Chloride penetration depth measurement

After being subjected to chloride for a certain period of time, ECC specimens were taken out and cut in the direction perpendicular to the crack plane with no water. The freshly cut surface was treated by 0.1 mol/L $AgNO_3$ solution as a chloride color indicator. The area with existence of free chlorides (at least approximately 0.15 % by weight of cement [37]) would turn into white while the area with no chloride or low chloride content shall become brown. The chloride penetration depth was measured by a caliper. Considering the symmetry of specimens, only one side of the specimen was measured. As shown in Fig. 1, the measurement started from the edge that is away from the crack of 20 mm. The interval of measurement was 2 mm away from the crack of 4 mm. Within the area close to the crack, the interval gradually decreases with the distance to the crack becoming smaller. They are 1 mm, 0.5 mm and 0.25 mm, see Fig. 1. Note that for reference (i.e. uncracked) specimens, a constant interval of 2 mm was used.

2.4. Chloride content measurement

The change of total amount of chloride and water-soluble chloride perpendicular to the exposure surface was measured as shown in Fig. 1. The specimen was sliced and sampled by a cutting machine along the crack. The slice has a width of about 10 mm (i.e., 5 mm to both sides of

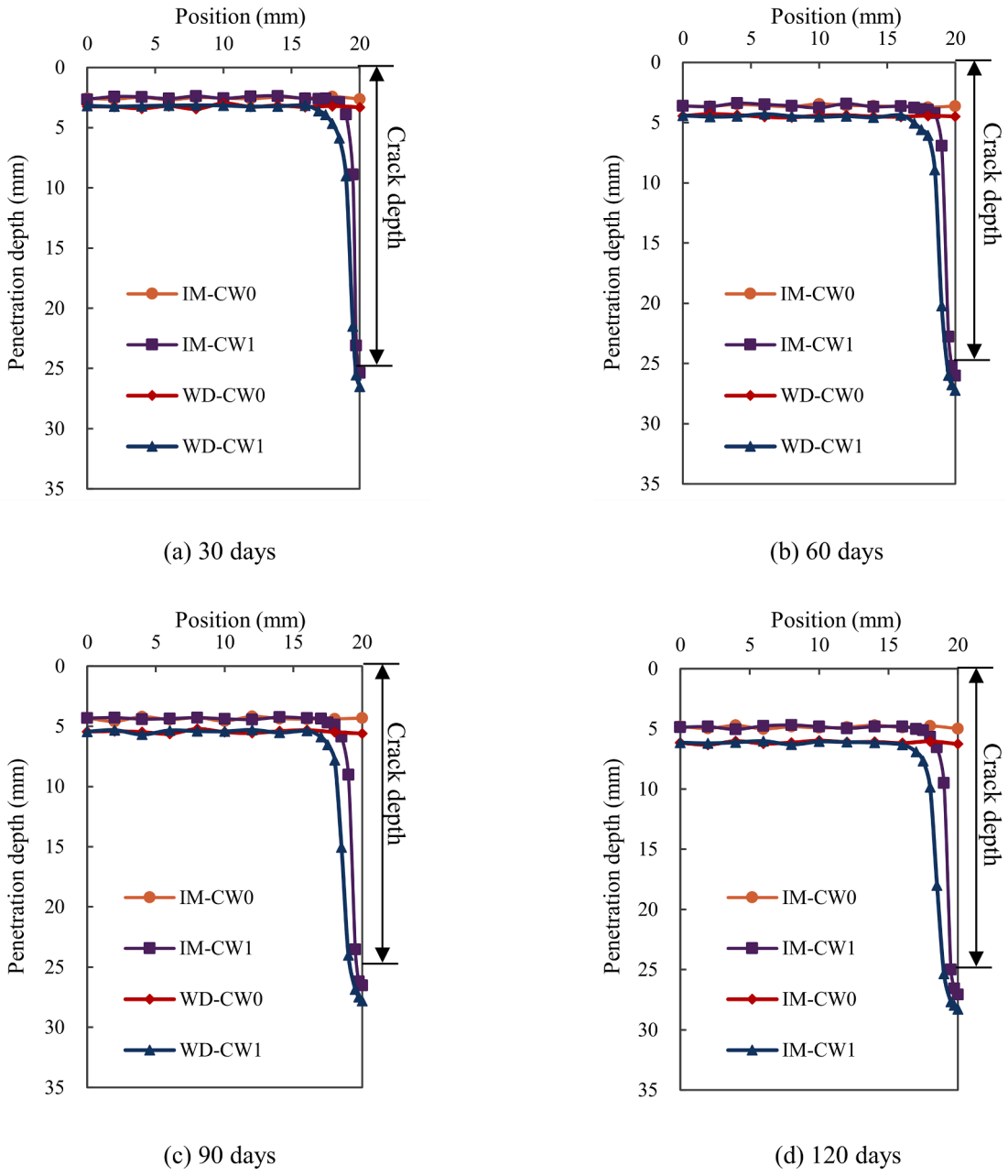

Fig. 5. Chloride penetration profile of specimens under immersion and wet/dry cycles.

the crack). The thickness of the slice changed along the depth where it was cut from. Their corresponding depths were 0–2 mm, 2–4 mm, 4–7 mm, 7–10 mm, 10–15 mm, 15–20 mm, 20–25 mm, and 25–30 mm, respectively. The slices were crushed and ground into a powder. A 0.3 mm sieve was used to sieve the powders. The remaining powders were oven-dried under 60 °C for 24 h. In terms of the water-soluble chloride measurement, 2 g of powder was dissolved in 200 mL distilled water using magnetic stirrers. After 30 min of mixing, the free chloride content test was measured using a NELD-CL420 chloride ion selective electrode. With respect to the total amount of chloride, dilute nitric acid (volume ratio of concentrated nitric acid and distilled water = 3:17) was used to dissolve the binding chlorides according to AASHTO T 260–97 [38]. The NELD-CL420 chloride ion selective electrode was then used to measure the chloride content. Specimens with no crack were used as reference.

2.5. XRD and MIP measurements

To reveal the change of mineral composition of different phases, porosity and pore size distribution under the aforementioned exposure conditions, small cubes with size of 5 mm next to the top of the crack

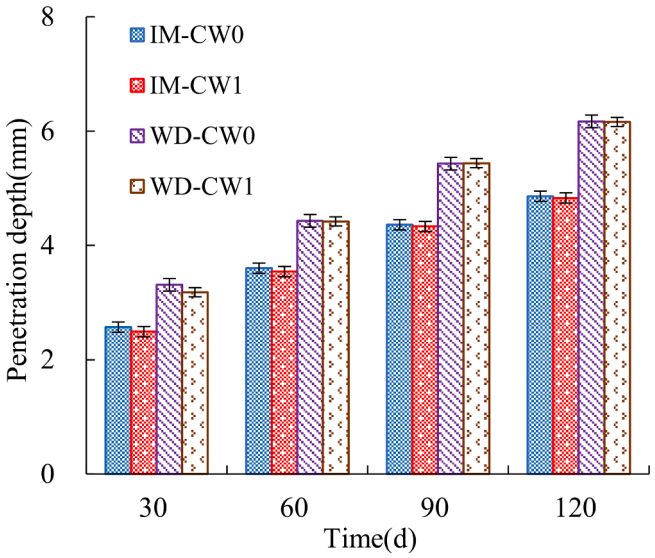

Fig. 6. Comparison of chloride penetration depth in uncracked area with or without wet-dry cycles.

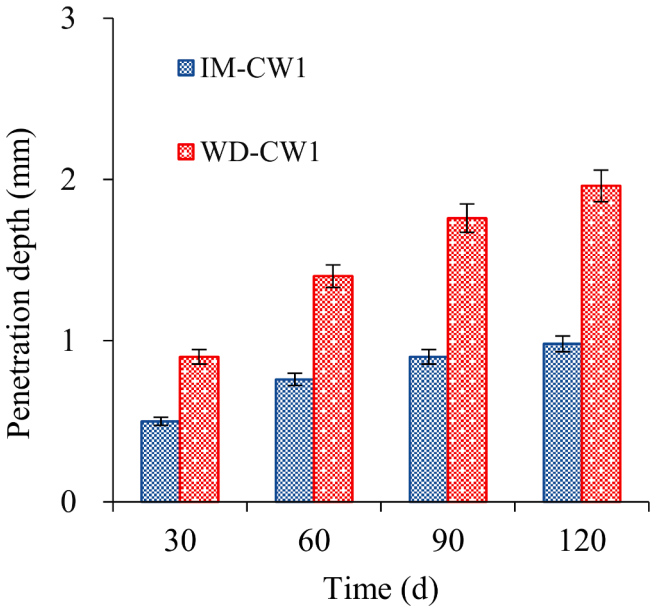

Fig. 7. Penetration depth perpendicular to the crack walls at depth of 10 mm.

(see Fig. 1) were cut out for the XRD and MIP analysis, respectively. Specimens soaked in water were used as reference. The exposure time was 60 and 120 days for all cases.

In terms of XRD, a PANalytical AERIS X-ray diffractometer was used. Prior to the test, the samples were dried in an oven at 60 °C for 24 h, ground, and sieved through 75 μm. The powders were dried in an oven at 45 °C for 48 h. The adopted Cu-Ka radiation has a voltage of 40 kV and current of 30 mA. The scanning speed was 0.02°/s for a range of 5–90°.

Regarding MIP, the collected samples were first immersed in isopropanol for 3 days. Afterwards, they were dried under 45 °Cfor 48 h using vacuum. An Autopore II 9220 mercury porosimeter was then used for the measurement. The adopted contact angle was 130°. The pressure capacity of the instrument is between 4×10^{-3} and 4.13×10^{2} MPa, corresponding to a pore size ranging from 7 nm to 314 μm.

3. Experimental results and discussion

3.1. Chloride penetration depth

3.1.1. Influence of crack width

Fig. 2 illustrates the mean chloride penetration profile of ECC under soaking conditions. Away from the crack, the penetration depth is

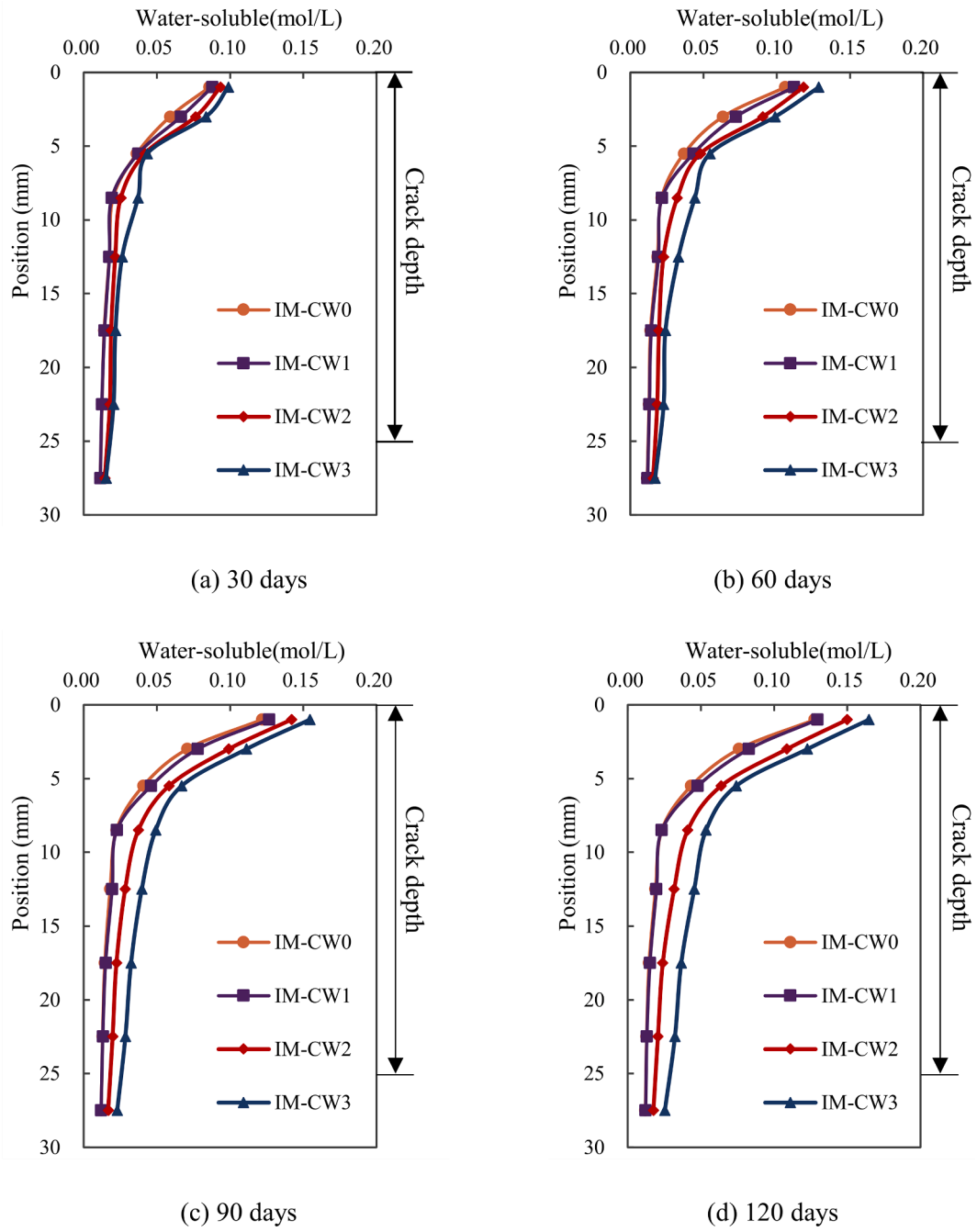

Fig. 8. Water-soluble chloride profile after different immersion period.

relatively constant. When the distance to crack decreases, an increase in penetration depth is observed as the chloride can ingress from both the crack wall and the top surface. This influence becomes more significant with increasing immersion time and crack width. Furthermore, the penetration depth perpendicular to the crack wall decreases along the crack depth and reach the minimum value at the end of the crack. Remarkable increment of the penetration is observed at the end when the crack width increases from 0.1 mm to 0.2 mm. This is in accordance with the plain concrete [39].

Fig. 3 shows the average penetration depth at the positions over 12 mm away from the crack. At the same immersion period, the difference among all cases is within 5 %. This means that the crack width has no influence on the chloride ingress in this area. The penetration depth increases with the immersion time. It is 2.57 mm at 30 days, and gradually increases to 3.61 mm, 4.34 mm and 4.84 mm at 60, 90 and 120 days, respectively. The increments are 40.5 %, 20.2 %, and 11.5 % for every 30 days interval. The significant decrease in the chloride ingress can be attributed to the densification of the microstructure

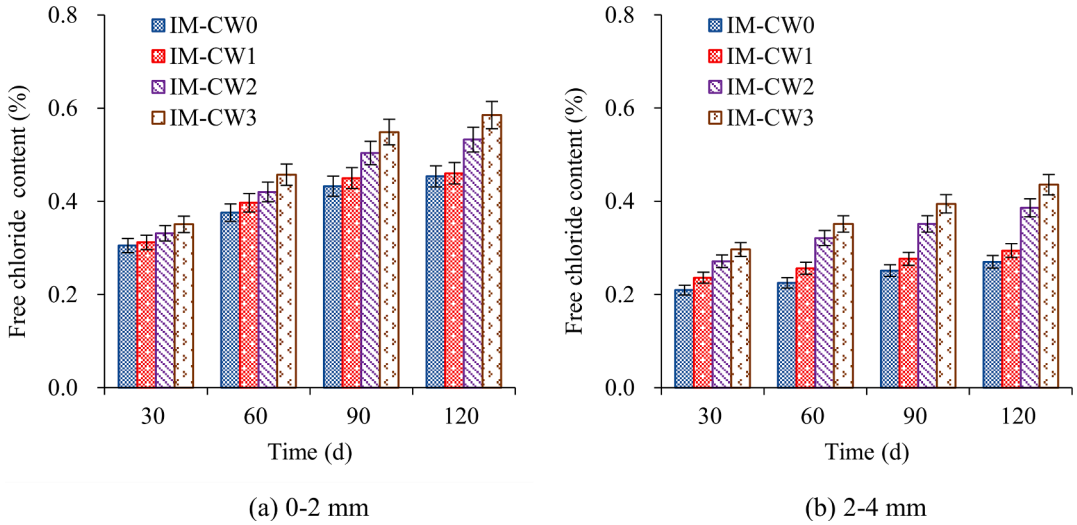

Fig. 9. Water-soluble chloride content at depths of 0–2 mm and 2–4 mm under immersion condition.

which is further discussed in Section 3.4.

The penetration depth perpendicular to the crack walls at crack depth of 10 mm is compared in Fig. 4. Regardless of the immersion time, the larger the crack, the higher the penetration depth is observed. After immersion of 30 days, the penetration depths were 0.50 mm, 1.46 mm, and 2.52 mm for specimens with crack width of 0.1 mm, 0.2 mm and 0.3 mm, respectively. The penetration depth of IM-CW3 and IM-CW2 are about 2.92 and 5.04 times of IM-CW1. Note that the penetration depth of IM-CW3 at this crack depth is very close to that of the exposed surface. This observation remained unchanged with the exposure time increasing. Therefore, 0.3 mm can be regarded as the upper threshold crack width of ECC. Furthermore, with exposure time increasing, the difference between IM-CW3 and IM-CW2 decreased while opposite trend is obtained for IM-CW2 and IM-CW1. After 90 days exposure, the chloride ingress rate is significantly reduced, which is possibly attributed to the self-healing behavior of such material which is more prominent in small cracks [40–42].

3.1.2. Influence of wet-dry cycles

Fig. 5 shows the influence of wet-dry cycles on the chloride penetration profile of uncracked and cracked specimens at various exposure period. Clearly, the chloride penetration depth is significantly increased at all the tested positions, especially at the area influenced by both the crack wall and the flat surface. The difference between the two exposure conditions becomes more obvious with exposure duration. This can be attributed to the fact that the wet-dry cycles combine both the sorption and diffusion, which induces a steep concentration gradient and amplifies the diffusion rate [43]. Furthermore, in cracks, capillary suction plays a more important role when the concrete is unsaturated, making the penetration of moisture (and associated ions) much faster [44].

The average chloride penetration depth at the region away from the crack is shown in Fig. 6. Clearly, the crack has no influence on this area. Different with immersion condition, the increment rate of penetration depth under wet-dry at does not significantly change with the exposure period. It is increased by 28.8 %, 25.1 %, 24.5 % and 27.0 % with each 30 days interval.

The penetration depth perpendicular to the crack walls at crack depth of 10 mm with and without wet-dry cycles is compared in Fig. 7. With exposed period increasing, the difference between the two exposure conditions become more significant. The penetration depths are 0.5 mm, 0.76 mm, 0.90 mm, and 0.98 mm under immersion conditions at 30, 60, 90 and 120 days. Under wet-dry cycles, the penetration depth is increased by 80.0 %, 84.2 %, 95.6 % and 100 % at the corresponding exposure periods. The increment is more significant than the sounded area.

3.2. Water-soluble chloride content

3.2.1. Influence of crack width

Fig. 8 shows the influence of crack width on the water-soluble chloride content profile along the crack depth. Similar to the chloride penetration depth, the water-soluble chloride content increases with an increasing crack width. The water-soluble chloride content profile of IM-CW0 and IM-CW1 is more or less the same. This implies that a 0.1 mm crack in ECC has limited effect on the chloride ingress in ECC under immersion condition. When the crack width increases to 0.2 mm, a significant increase is observed. Therefore, 0.1 mm can be regarded as the lower threshold of crack width.

Fig. 9 shows the water-soluble chloride content versus diffusion time at the depths of 0–2 mm and 2–4 mm. Clearly, the influence of the crack becomes more obvious with the increase of crack width. The water-soluble chloride content of ECC without the crack was 0.305 % in depth of 0–2 mm at 30 days. An increase of 2.3 %, 8.5 % and 14.8 % is found for IM-CW1, IM-CW2, IM-CW3 respectively. In the depth of 2–4 mm, the water-soluble chloride content of IM-CW1, IM-CW2, IM-CW3 is 0.236 %, 0.271 % and 0.297 %, 12.9 %, 29.7 % and 42.1 % greater than the integrated ECC (0.209 %) respectively. Furthermore, the effect of crack width on the chloride content becomes more obvious with increasing time. The changes in water-soluble chloride content are particularly prominent when the crack width is>0.2 mm. An increase of 8.7 % and 14.9 % is observed for IM-CW2 and IM-CW3 compared to that of IM-CW0 at depth of 0–2 mm. These increments reach 17.4 % and 29.4 % respectively at 120 days. In terms of 2–4 mm, increment of 29.5 % and 41.6 % is observed for IM−CW2 and IM-CW3 compared to that of IM-CW0 at 30 days. They become 42.9 % and 61.2 %, respectively at 120 days.

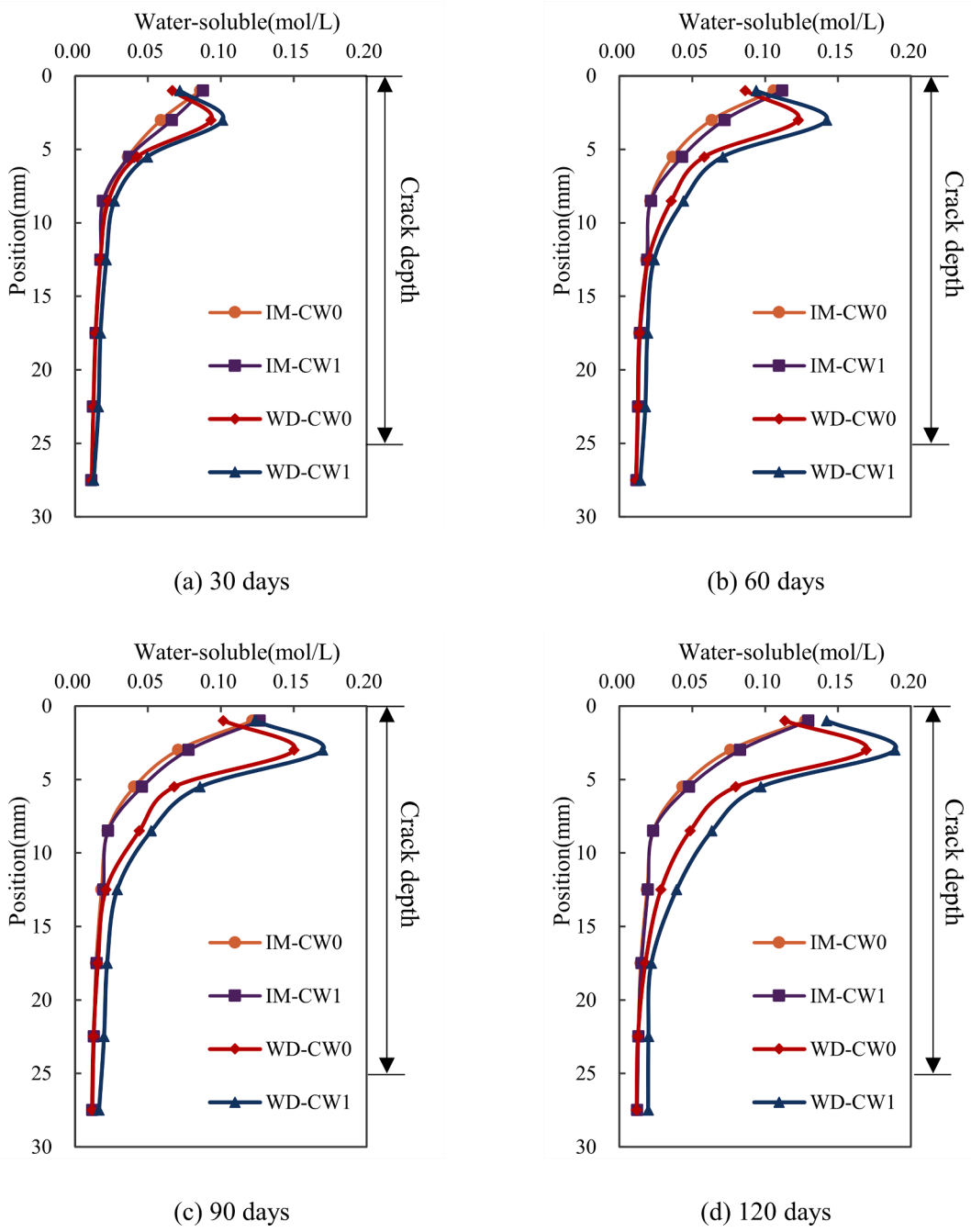

Fig. 10. Comparisons of water-soluble chloride profile under immersion and wet-dry cycles.

3.2.2. Influence of wet-dry cycles

Fig. 10 compares the water-soluble chloride content profile of specimens under immersion and wet-dry cycles. Unlike the immersion condition, chloride content first increases to the maximum and then decreases with depth increasing, which is generally termed as the "maximum phenomenon"[45,46]. It is the rapid accumulation of chlorides at a certain depth caused by the coupled effects of capillary adsorption and water evaporation during the wet-dry cycles [47,48]. It seems that the depth at which the maximum chloride content appears (d_{Cmax}) remains in the depth of 2–4 mm regardless of the crack width and exposure time, while the maximum content increases with the exposure time. The existence of the crack further stimulates such influence. Compared with the reference specimen, the maximum chloride content increases by 8.57 %, 15.94 %, 12.75 % and 11.52 % for 30, 60, 90 and 120 days, respectively.

For the reference specimen, the chloride content at depth smaller than d_{Cmax} is less than that of the immersion condition. When the 0.1 mm crack is introduced, this phenomenon does not exist after 90 d as the

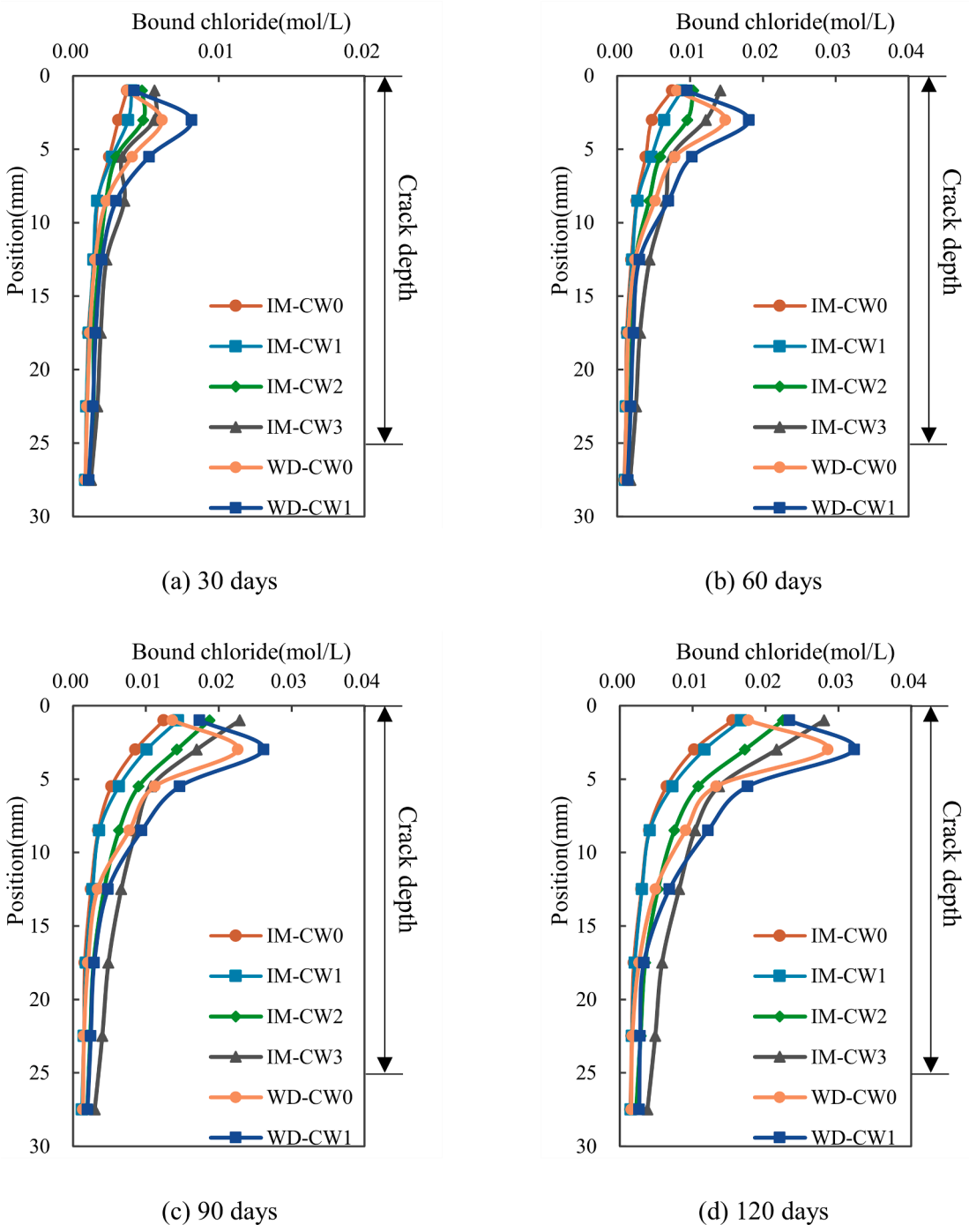

Fig. 11. Bound chloride profile under immersion and wet-dry cycles.

wet-dry cycles promote the chloride ingress perpendicular to the crack wall. Furthermore, it seems that, beyond a certain depth, the chloride content of IM-CW0, IM-CW1 and WD-CW0 remains the same, although this depth is enlarged with the exposure period. In terms of WD-CW1, the water-soluble chloride content is always higher than the other cases. This become more remarkable with exposure period increasing. In this case, the lower crack width threshold does not exist or become much smaller.

3.3. Chloride ion binding isotherm

The bound chloride ion content is calculated as the difference between total chloride ion and water-soluble chloride ion content. The profile of bound chloride content along the crack is shown in Fig. 11. Clearly, the bound chloride ion profile has a similar trend with the water-soluble chloride ion. With exposure time increasing, the bound chloride content keeps increasing. Under immersion conditions, the

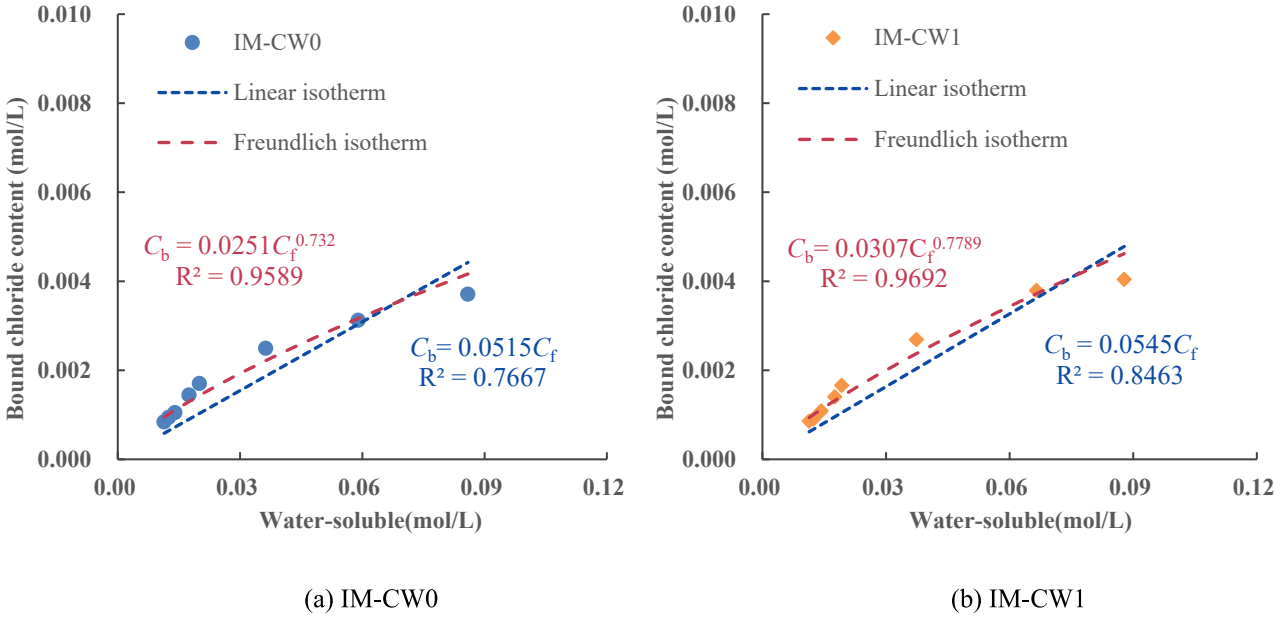

Fig. 12. Chloride ions binding isotherms of different cases after 30 days exposure.

bound chloride decreases with the crack depth. The larger the crack width, the higher the bound chloride content is observed. Furthermore, the increment of crack width from 0.1 mm to 0.2 mm leads to more significant change of the bound chloride content profile. The "maximum phenomenon" occurs for the wet-dry cycles. Different with the water-soluble chloride ion, the bound chloride ion content at depth smaller than d_{Cmax} is larger than the immersion condition. This means that ECC possesses a higher chloride ion binding capacity under wet-dry cycles than immersion conditions. This is in accordance with the observation in concrete [49,50].

The relationship between free and bound chloride ions over a range of chloride concentrations at a given temperature is known as the binding isotherm. Both linear and nonlinear chloride binding isotherms have been proposed [34]. The linear binding isotherm is generally expressed as Eq. (1):

$$C_b = aC_f \tag{1}$$

where C_b is the bound chloride content, C_f the water-soluble chloride content, a is a constant that can be fitted by experimental data. For the nonlinear isotherms, Langmuir and Freundlich are the mostly applied. Tang and Nilsson [51] showed that the Freundlich isotherm is more suitable when the free chloride concentration is in the range of 0.01 to 1 M. The equation as expressed following was used.

$$C_b = \alpha C_f^{\beta} \tag{2}$$

where α and β are the Freundlich constants.

Fig. 12 shows the fitted Linear and Freundlich isotherms after 30 days exposure. Clearly, Freundlich isotherm shows high determination coefficient (>0.93) for all cases. The determination coefficient of the linear model is smaller than 0.9. In terms of IM-CW0, it is as low as 0.7667. Therefore, it is more suitable to use the Freundlich isotherm to represent the chloride binding behavior of studied ECC. Table 4 shows the fitted Freundlich constants for all exposure periods. As can be seen from the table that determination coefficient remains high (>0.93) for all cases. With exposure period increasing, value of α and β also increase. This means that more chloride ions are bound at a certain water-soluble chloride content after a relatively longer exposure period. Although it is generally believed that the chloride binding capacity is independent of exposure time, this is not the case in the current study as the test duration is not long enough [49]. Additionally, the binding capacity increases with crack width, as the crack promotes the ingress rate of chloride ions and it takes less time for the specimens with larger crack to reach a certain concentration of chloride ion. When wet-dry cycles are applied, α and β are higher than that of the immersion condition. As expected, more bound chloride ions are observed in the specimens under wet-dry cycles at the same water-soluble chloride content compared with those under immersion condition. This is in accordance with the observation in [49].

3.4. XRD and MIP

3.4.1. XRD

XRD pattern of ECC samples subjected to different conditions is depicted in Fig. 13. The diffraction peak at 2θ of 11.2° corresponds to Friedel's salt. Since quartz sand is used in ECC, quartz diffraction peaks are observed. The variation of the crystal phase mainly lies in Friedel's salt, portlandite, and calcite. After being soaked in water for 60 days, the intensity of peak corresponding to portlandite decreases significantly. This can be attributed to the pozzolanic reaction of the fly ash and dissolution of portlandite [52].

Obvious Friedel's salt diffraction peak appears after exposed to NaCl solution for 60 days. It becomes stronger with the crack width increasing. The wet-and-dry cycles strengthen the peak of Friedel salt for both cracked and integrated specimens. With the increase of exposure time the influence of crack and wet-and-dry cycles become more

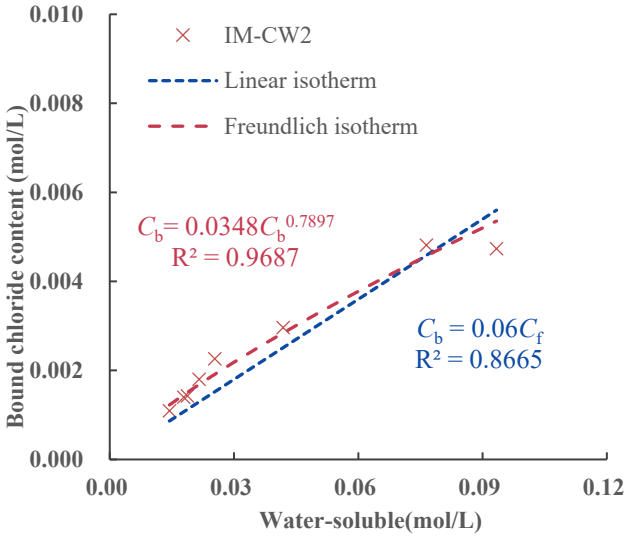

(c) IM-CW2

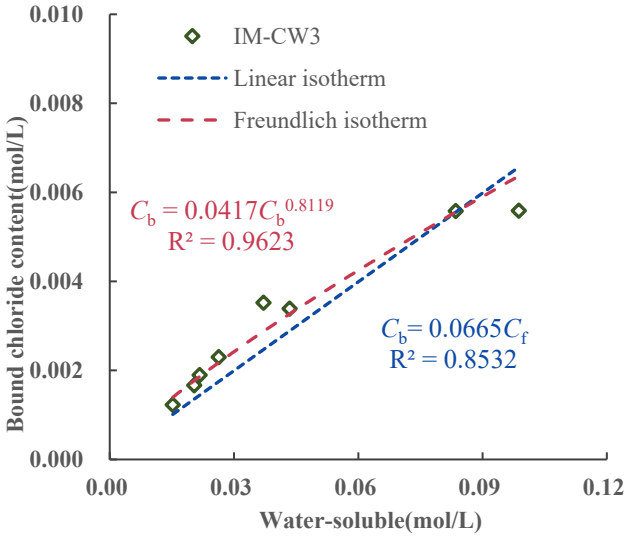

(d) IM-CW3

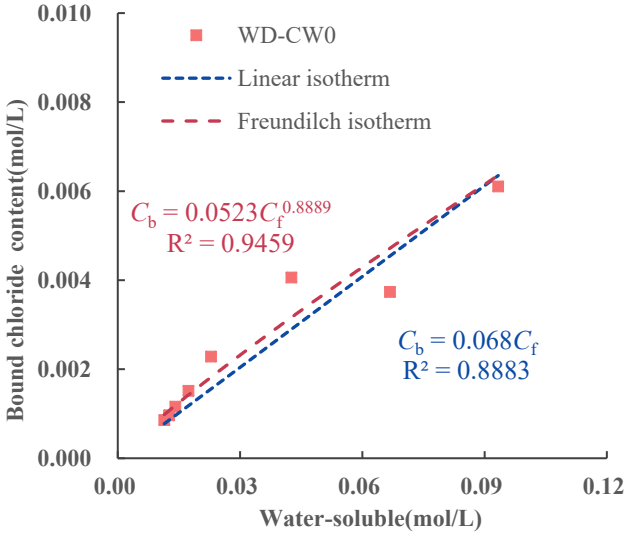

(e) WD-CW0

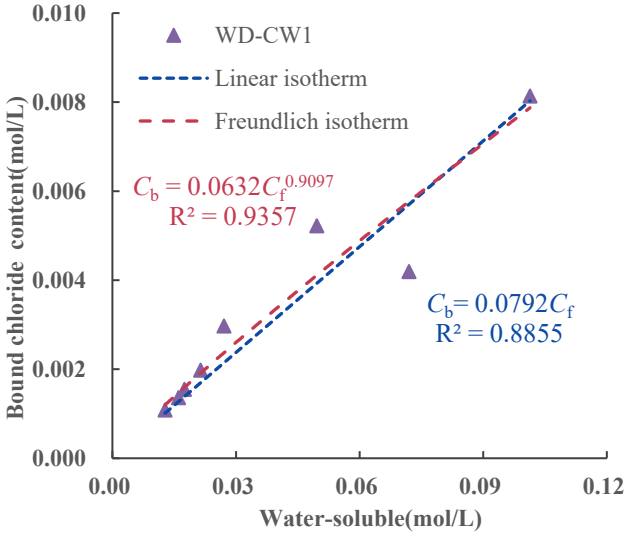

(f) WD-CW1

Fig. 12. (*continued*).

significant. The same trend is observed for calcite. Furthermore, the diffraction peak of Portlandite becomes much smaller in the integrated specimen after 60 days exposure and disappears after another 60 days exposure. When cracked specimens were subjected to wet-dry cycles, no Portlandite was observed. This is attributed to the reaction between tricalcium aluminate and chloride ions, which generates Friedel's salt. In this process, CO_3^{2-} are released from AFm, which further reacts with portlandite to form calcite [53–55]. Meanwhile, another reason for the reduction of portlandite is carbonization, which also generates calcite [56]. These products densify the microstructure, thus decreasing the porosity of the ECC as revealed in section 3.4.2. This leads to the reduction of the chloride ingress rate. For a quantitative study, the approach proposed in Ref [57].

3.4.2. MIP

The change of porosity and pore size distribution of ECC under various exposure conditions is shown in Fig. 14 and Fig. 15. It can be seen that, after 60 days water immersion, the porosity of ECC decreases from 6.57 % to 6.05 %. Pores > 10 μm and < 0.1 μm are reduced. Porosity further decreases to 5.70 % with another 60 days immersion. At

Table 4
Fitting results of Freundlich isotherm.

Erosion time/d	IM-CW0			IM-CW1		
	α	β	R^2	α	β	R^2
30	0.0251	0.7320	0.9589	0.0307	0.7789	0.9692
60	0.0595	0.8767	0.9530	0.0773	0.9317	0.9698
90	0.1116	0.9784	0.9739	0.1373	1.0256	0.9766
120	0.1338	0.9928	0.9771	0.1427	1.0026	0.9822
Erosion time/d	**IM-CW2**			**IM-CW3**		
	α	**β**	**R^2**	**α**	**β**	**R^2**
30	0.0348	0.7897	0.9687	0.0417	0.8119	0.9623
60	0.1000	0.9792	0.9674	0.1298	1.0124	0.9668
90	0.1707	1.0661	0.9792	0.1733	1.0431	0.9833
120	0.1868	1.0623	0.9846	0.2103	1.0755	0.9876
Erosion time/d	**WD-CW0**			**WD-CW1**		
	α	**β**	**R^2**	**α**	**β**	**R^2**
30	0.0523	0.8889	0.9459	0.0632	0.9097	0.9357
60	0.1360	1.0483	0.9764	0.1524	1.0702	0.9705
90	0.1896	1.0860	0.9857	0.1943	1.0907	0.9823
120	0.2011	1.0764	0.9932	0.2124	1.0916	0.9921

this period, pores in the size range of 0.1 and 10 μm turns into smaller sizes. The reduction in porosity is mainly attributed to the prolonged hydration of cement and pozzolanic reaction of fly ash, as revealed in section 3.4.1. When chloride exposure condition is introduced, the porosity is further reduced. This is attributed to the formation of calcite and Friedel's salt [58]. It seems like the crack with width of 0.1 mm does not significantly influence the porosity in the tested area. The reduction in porosity is more significant in specimens with cracks wider than 0.2 mm. Their porosities are 5.06 % and 4.64 % after 60 days of soaking, respectively. Compared with water immersion condition, the reduction ratios are 16.4 % and 23.3 % for IM-CW2 and IM-CW3, respectively. A more remarkable change is found for 120 days immersion. The porosity of IM-CW1, IM-CW2 and IM-CW3 reduces to 4.99 %, 4.45 % and 3.95 % respectively, which are 12.46 %, 21.93 % and 30.7 % smaller than that of the water immersion condition. This indicates that the influence of crack width on chloride ingress becomes more significant as the time increases.

Under wet-dry cycle condition, porosity of WD-CW0 and WD-CW1 are respectively 5.11 % and 4.83 % at 60 days, and respectively 4.53 % and 4.21 % at 120 days. At each exposure duration, the porosity is smaller than that of the specimen without wet-dry cycles. Note that pores smaller than 0.1 μm are significantly increased after 60 days exposure, which may promote capillary suction. It tends to confirm that the wet-dry cycles accelerate the chloride transport and promotes the binding of chlorides, resulting in a greater filling in the micropores. The reduction of porosity is proportional to the measured chloride content although the reduction in porosity slows down the chloride ingress rate. For example, after 120 days exposure, the porosity of IM-CW3 is reduced by 23.3 % compared to that of IM-CW0, while the maximum chloride content is increased by 29.0 %. And the porosity of WD-CW1 decreased by 15.6 % compared to IM-CW1, while the maximum chloride content increased by 45.7 %.

It should be emphasized here that the influence of addition of PVA fibers in cementitious materials on the resistance to chloride ion ingress is complex. On the one hand, fibers can block the connective pores, reducing the connectivity and reducing the permeability. On the other hand, the interface between fiber and matrix provides channels for the entry of chloride ions [59]. The compromise is mainly related to the amount and quality of used fly ash [60–62].

4. Conclusions

In this paper, influence of crack width and wet-dry cycles on the chloride ingress in ECC was investigated. It can provide a reference for the design of hybrid ECC concrete system, especially on the thickness of the layered ECC and life predictions. The following conclusions can be drawn.

The chloride penetration depth perpendicular to the crack wall increases with the crack width and decreases with the depth. Under immersion condition, the lower threshold of crack width of ECC material is about 0.1 mm and the upper threshold is about 0.3 mm. A significant reduction in chloride ingress rate is observed when crack width is smaller than 0.1 mm. However, when the wet-dry cycles are applied, the lower threshold crack width would be much finer. It should be noted that the width of the previously mentioned cracks is unchanged along the depth.

The "maximum phenomenon" is observed for both water-soluble and bound chloride ions profiles under wet-dry cycles. Compared with bound chloride ions, more reduction occurs for the water-soluble chloride ions at depth smaller than the one corresponding to maximum chloride content.

Freundlich isotherm can be used to describe the influence of the crack width and wet-dry cycles on the chloride binging isotherm. Both the crack width and wet-dry cycles increase the bound chloride ion content at the same water-soluble chloride content within the exposure period of 120 days.

The change of the mineral phases and porosity is related with the chloride binding behavior. Both the crack width, wet-dry cycles and

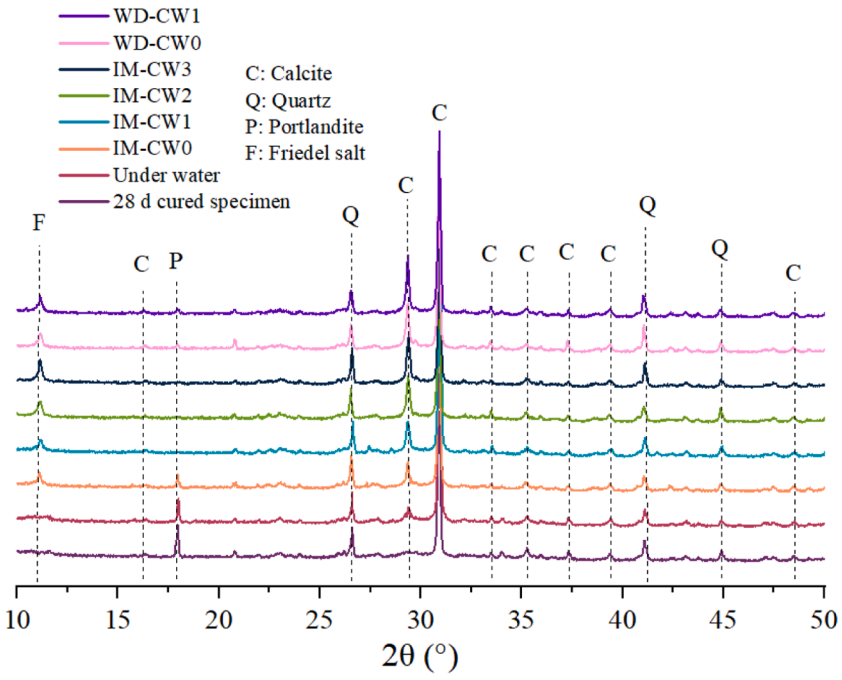

(a) 60 days

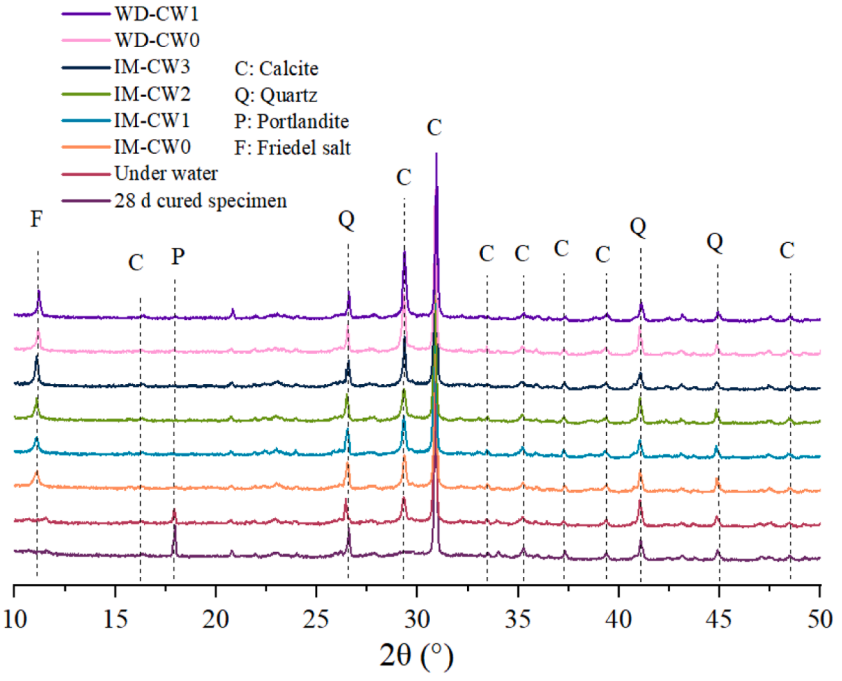

(b) 120 days

Fig. 13. XRD patterns of ECC specimens after 60 and 120 exposure.

exposure period refines the pore structure in the vicinity of the crack.

CRediT authorship contribution statement

Renjuan Sun: Methodology, Supervision, Writing – review & editing. **Wei Lu:** Investigation, Writing – original draft. **Chuanyi Ma:** Funding acquisition. **Abdullah M. Tawfek:** Methodology. **Yanhua Guan:** Writing – review & editing. **Xinlei Hu:** Investigation, Methodology. **Hongzhi Zhang:** Writing – review & editing. **Yifeng Ling:** Methodology, Writing – review & editing. **Branko Šavija:** Methodology, Writing – review & editing.

Work condition	28 d cured specimen	Under water	IM-CW0	IM-CW1	IM-CW2	IM-CW3	WD-CW0	WD-CW1
Porosity (%)	6.57	6.05	5.62	5.48	5.06	4.64	5.11	4.83

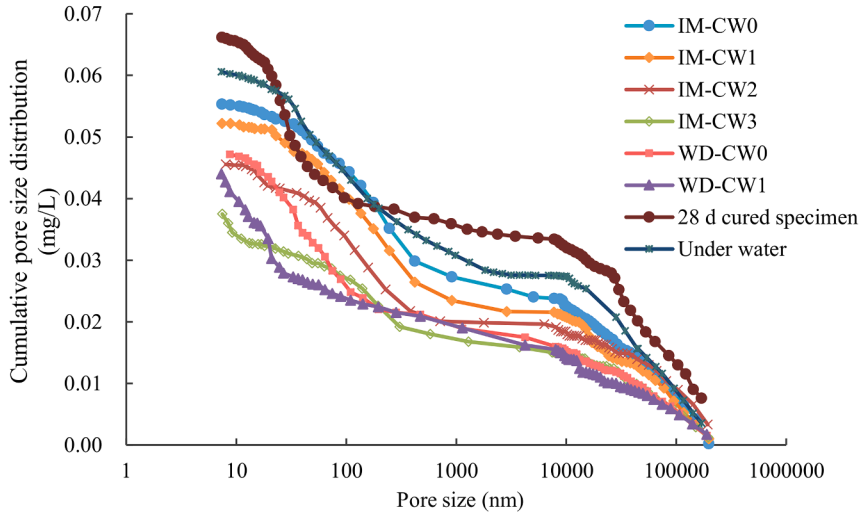

(a) 60 days

Work condition	28 d cured specimen	Under water	IM-CW0	IM-CW1	IM-CW2	IM-CW3	WD-CW0	WD-CW1
Porosity (%)	6.57	5.70	5.15	4.99	4.45	3.95	4.53	4.21

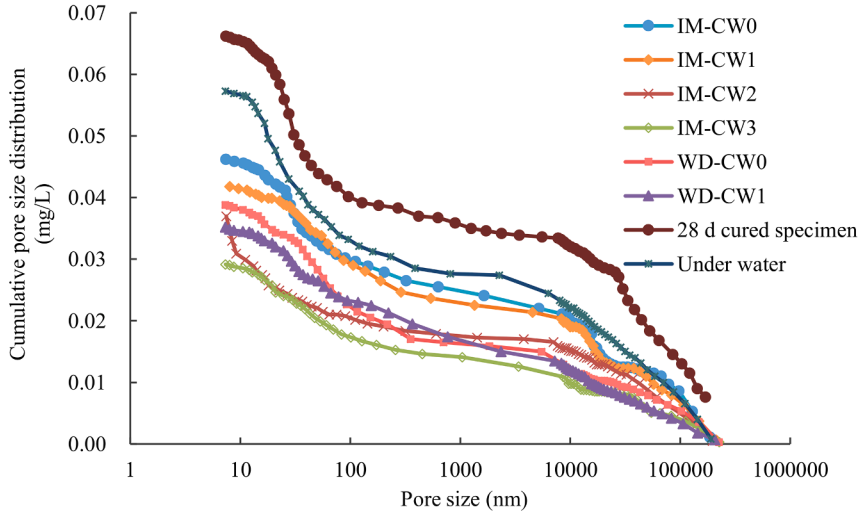

(b) 120 days

Fig. 14. Cumulative pore size distribution of ECC under different exposure conditions.

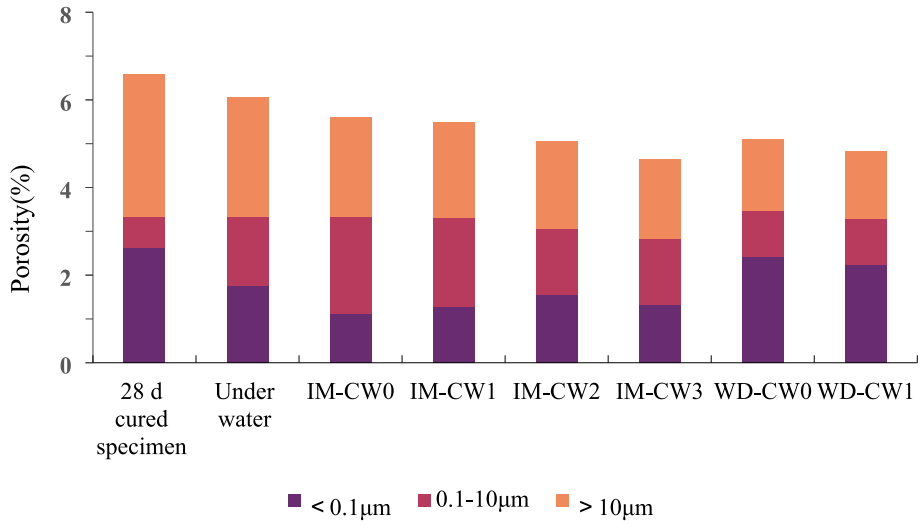

(a) 60 days

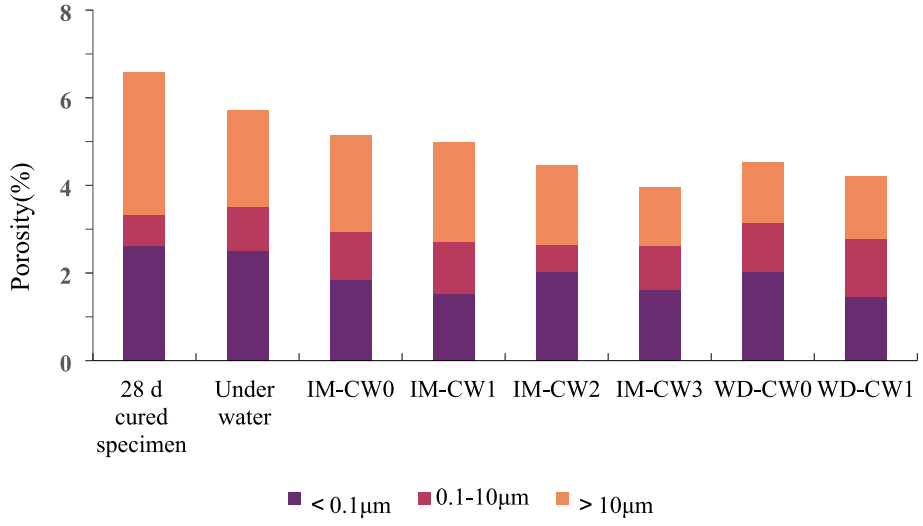

(b) 120 days

Fig. 15. Pore size distribution of ECC under different exposure conditions.

Declaration of Competing Interest

The authors declare that they have no known competing financial interests or personal relationships that could have appeared to influence the work reported in this paper.

Data availability

Data will be made available on request.

Acknowledgements

This work was supported by the National Natural Science Foundation of China (No. 52008234), Taishan Scholars Foundation of Shandong Province (No. tsqn201909032), Natural Science Foundation of Jiangsu Province (No. BK20200235) and Natural Science Foundation of Shandong Province (ZR2021QE174, ZR2021ME215).

References

[1] G.P. Tilly, J. Jacobs, Concrete repairs: Observations on performance in service and current practice, Watford, UK (2007).
[2] L. Bertolini, Steel corrosion and service life of reinforced concrete structures, Struct. Infrastruct. E. 4 (2) (2008) 123–137.
[3] R.E. Melchers, Modelling durability of reinforced concrete structures, Corros. Eng., Sci. Technol. 55 (2) (2020) 171–181.
[4] C. Arya, S. Bioubakhsh, P. Vassie, Chloride penetration in concrete subject to wet/dry cycling: influence of moisture content, P. I, Civil Eng.-Str. B. 167 (2) (2014) 94–107.
[5] L. Chunhua, L. Ronggui, C. Zhaowei, Y. Yongdong, Study on chloride penetration into flexural cracked reinforced concrete beams subjected to drying-wetting cycles, China Civ. Eng. J. (2014).
[6] C. Lu, Y. Gao, Z. Cui, R. Liu, Experimental analysis of chloride penetration into concrete subjected to drying–wetting cycles, J. Mater. Civil Eng. 27 (12) (2015) 4015036.

[7] C. Lu, R. Liu, Z. Cui, Y. Gao, Chloride Diffusion Model in Cracked Fly Ash Concrete Bridge Subjected to Coastal Drying-wetting Cycles, China J. Highway Transp. 28 (8) (2015) 40–49.
[8] R. Sun, X. Hu, Y. Ling, Z. Zuo, P. Zhuang, F. Wang, Chloride diffusion behavior of engineered cementitious composite under dry-wet cycles, Constr. Build. Mater. 260 (2020), 119943, https://doi.org/10.1016/j.conbuildmat.2020.119943.
[9] P. Gao, Y. Chen, H. Huang, Z. Qian, E. Schlangen, J. Wei, Q. Yu, Investigation of drying-induced non-uniform deformation, stress, and micro-crack propagation in concrete, Cem. Concr. Compos. 114 (2020), 103786.
[10] J. Peng, S. Hu, J. Zhang, C.S. Cai, L. Li, Influence of cracks on chloride diffusivity in concrete: A five-phase mesoscale model approach, Constr. Build. Mater. 197 (2019) 587–596.
[11] B. Šavija, E. Schlangen, J. Pacheco, S. Millar, T. Eichler, G. Wilsch, Chloride ingress in cracked concrete: a laser induced breakdown spectroscopy (LIBS) study, J. Adv. Concr. Technol. 12 (10) (2014) 425–442.
[12] A. Djerbi, S. Bonnet, A. Khelidj, V. Baroghel-Bouny, Influence of traversing crack on chloride diffusion into concrete, Cem. Concr. Res. 38 (6) (2008) 877–883.
[13] S.Y. Jang, B.S. Kim, B.H. Oh, Effect of crack width on chloride diffusion coefficients of concrete by steady-state migration tests, Cem. Concr. Res. 41 (1) (2011) 9–19.
[14] Y. Li, X. Chen, L. Jin, R. Zhang, Experimental and numerical study on chloride transmission in cracked concrete, Constr. Build. Mater. 127 (2016) 425–435.
[15] M. Ismail, A. Toumi, R. François, R. Gagné, Effect of crack opening on the local diffusion of chloride in inert materials, Cem. Concr. Res. 34 (4) (2004) 711–716, https://doi.org/10.1016/j.cemconres.2003.10.025.
[16] K. Wang, D.C. Jansen, S.P. Shah, A.F. Karr, Permeability study of cracked concrete, Cem. Concr. Res. 27 (3) (1997) 381–393.
[17] H. Wang, J. Dai, X. Sun, X. Zhang, Characteristics of concrete cracks and their influence on chloride penetration, Constr. Build. Mater. 107 (2016) 216–225, https://doi.org/10.1016/j.conbuildmat.2016.01.002.
[18] S. Mu, G. De Schutter, B.G. Ma, Non-steady state chloride diffusion in concrete with different crack densities, Mater. Struct./Materiaux et Constructions. 46 (1–2) (2013) 123–133, https://doi.org/10.1617/s11527-012-9888-0.
[19] H. Ye, N. Jin, X. Jin, C. Fu, Model of chloride penetration into cracked concrete subject to drying–wetting cycles, Constr. Build. Mater. 36 (2012) 259–269, https://doi.org/10.1016/j.conbuildmat.2012.05.027.
[20] L. Wei, Y. Wang, J. Yu, J. Xiao, S. Xu, Feasibility study of strain hardening magnesium oxychloride cement-based composites, Constr. Build. Mater. 165 (2018) 750–760, https://doi.org/10.1016/j.conbuildmat.2018.01.041.
[21] V.C. Li, On engineered cementitious composites (ECC) a review of the material and its applications, J. Adv. Concr. Technol. 1 (3) (2003) 215–230.
[22] H. Liu, Q. Zhang, C. Gu, H. Su, V.C. Li, Influence of micro-cracking on the permeability of engineered cementitious composites, Cem. Concr. Compos. 72 (2016) 104–113.
[23] M. Sahmaran, M. Li, V.C. Li, Transport properties of engineered cementitious composites under chloride exposure, ACI Mater. J. 104 (6) (2007) 604–611.
[24] S. Miyazato, Y. Hiraishi, Transport properties and steel corrosion in ductile fiber reinforced cement composites, 2005, pp. 20-25.
[25] S. Zhuang, Q. Wang, Inhibition mechanisms of steel slag on the early-age hydration of cement, Cem. Concr. Res. 140 (2021), 106283.
[26] M. Maalej, V.C. Li, Introduction of strain-hardening engineered cementitious composites in design of reinforced concrete flexural members for improved durability, Struct. J. 92 (2) (1995) 167–176.
[27] B. Huang, Q. Li, S. Xu, L. Zhang, Static and fatigue performance of reinforced concrete beam strengthened with strain-hardening fiber-reinforced cementitious composite, Eng. Struct. 199 (2019), 109576.
[28] S. Mustafa, S. Singh, D. Hordijk, E. Schlangen, M. Luković, Experimental and numerical investigation on the role of interface for crack-width control of hybrid SHCC concrete beams, Eng. Struct. 251 (2022), 113378.
[29] M. Luković, D.A. Hordijk, Z. Huang, E. Schlangen, Strain Hardening Cementitious Composite (SHCC) for crack width control in reinforced concrete beams, Heron. 64 (1/2) (2019) 181.
[30] Y. Guan, H. Yuan, Z. Ge, Y. Huang, S. Li, R. Sun, Flexural properties of ECC-concrete composite beam, Adv. Civ. Eng. 2018 (2018) 1–7.
[31] Y. Guan, J. Wu, R. Sun, H. Zhang, Y. Hu, F. Wang, Transverse Flexural Behaviour of Steel-Engineering Cementitious Composites (ECC) Composite Deck under Negative and Positive Bending Forces, KSCE J. Civ. Eng. 25 (8) (2021) 2962–2973.
[32] H. Huang, X. Gao, L. Teng, Fiber alignment and its effect on mechanical properties of UHPC: An overview, Constr. Build. Mater. 296 (2021) 123741.
[33] K. Kobayashi, D. Le Ahn, K. Rokugo, Effects of crack properties and water-cement ratio on the chloride proofing performance of cracked SHCC suffering from chloride attack, Cem. Concr. Compos. 69 (2016) 18–27.
[34] K. Kobayashi, Y. Kojima, Effect of fine crack width and water cement ratio of SHCC on chloride ingress and rebar corrosion, Cem. Concr. Compos. 80 (2017) 235–244.
[35] R. Sun, L. Han, H. Zhang, Z. Ge, Y. Guan, Y. Ling, E. Schlangen, B. Šavija, Fatigue life and cracking characterization of engineered cementitious composites (ECC) under flexural cyclic load, Constr. Build. Mater. 335 (2022), 127465, https://doi.org/10.1016/j.conbuildmat.2022.127465.
[36] B. Qi, J. Gao, F. Chen, D. Shen, Chloride penetration into recycled aggregate concrete subjected to wetting–drying cycles and flexural loading, Constr. Build. Mater. 174 (2018) 130–137.
[37] N. Otsuki, S. Nagataki, K. Nakashita, Evaluation of AgNO 3 solution spray method for measurement of chloride penetration into hardened cementitious matrix materials, Mater. J. 89 (6) (1992) 587–592.
[38] T. Aashto, Standard method of test for sampling and testing for chloride ion in concrete and concrete raw materials. American Association of State Highway and Transportation Officials …, 2009.
[39] L. Marsavina, K. Audenaert, G. De Schutter, N. Faur, D. Marsavina, Experimental and numerical determination of the chloride penetration in cracked concrete, Constr. Build. Mater. 23 (1) (2009) 264–274.
[40] G. Yıldırım, Ö.K. Keskin, S.B. Keskin, M. Şahmaran, M. Lachemi, A review of intrinsic self-healing capability of engineered cementitious composites: Recovery of transport and mechanical properties, Constr. Build. Mater. 101 (2015) 10–21, https://doi.org/10.1016/j.conbuildmat.2015.10.018.
[41] S.Z. Qian, J. Zhou, E. Schlangen, Influence of curing condition and precracking time on the self-healing behavior of engineered cementitious composites, Cem. Concr. Compos. 32 (9) (2010) 686–693.
[42] B. Savija, E. Schlangen, Autogeneous healing and chloride ingress in cracked concrete, Heron 61 (1) (2016) 2016.
[43] M.Z.Y. Ting, K.S. Wong, M.E. Rahman, S.J. Meheron, Deterioration of marine concrete exposed to wetting-drying action, J. Clean. Prod. 278 (2021), 123383.
[44] B. Šavija, M. Luković, E. Schlangen, Influence of cracking on moisture uptake in strain-hardening cementitious composites, J. Nanomech. Micromech. 7 (1) (2017) 4016010.
[45] H. Chang, S. Mu, D. Xie, P. Wang, Influence of pore structure and moisture distribution on chloride "maximum phenomenon" in surface layer of specimens exposed to cyclic drying-wetting condition, Constr. Build. Mater. 131 (2017) 16–30.
[46] H. Chang, S. Mu, P. Feng, Influence of carbonation on "maximum phenomenon" in surface layer of specimens subjected to cyclic drying-wetting condition, Cem. Concr. Res. 103 (2018) 95–109.
[47] H. Ye, C. Fu, N. Jin, X. Jin, Influence of flexural loading on chloride ingress in concrete subjected to cyclic drying-wetting condition, Comput. Concrete. 15 (2) (2015) 183–198.
[48] J. Ožbolt, F. Oršanić, G. Balabanić, Modeling influence of hysteretic moisture behavior on distribution of chlorides in concrete, Cem. Concr. Compos. 67 (2016) 73–84.
[49] Y. Wang, C. Liu, Y. Tan, Y. Wang, Q. Li, Chloride binding capacity of green concrete mixed with fly ash or coal gangue in the marine environment, Constr. Build. Mater. 242 (2020), 118006.
[50] J. Zuquan, Z. Xia, Z. Tiejun, L. Jianqing, Chloride ions transportation behavior and binding capacity of concrete exposed to different marine corrosion zones, Constr. Build. Mater. 177 (2018) 170–183.
[51] T. Luping, L. Nilsson, Chloride binding capacity and binding isotherms of OPC pastes and mortars, Cem. Concr. Res. 23 (2) (1993) 247–253.
[52] Q. Zhu, L. Jiang, Y. Chen, J. Xu, L. Mo, Effect of chloride salt type on chloride binding behavior of concrete, Constr. Build. Mater. 37 (2012) 512–517.
[53] M. Florea, H. Brouwers, Chloride binding related to hydration products: Part I: Ordinary Portland Cement, Cem. Concr. Res. 42 (2) (2012) 282–290.
[54] F. Shaheen, B. Pradhan, Influence of sulfate ion and associated cation type on steel reinforcement corrosion in concrete powder aqueous solution in the presence of chloride ions, Cem. Concr. Res. 91 (2017) 73–86.
[55] D. Wang, Q. Wang, Z. Huang, New insights into the early reaction of NaOH-activated slag in the presence of CaSO4, Compos. B Eng. 198 (2020), 108207.
[56] H. Ye, X. Jin, C. Fu, N. Jin, Y. Xu, T. Huang, Chloride penetration in concrete exposed to cyclic drying-wetting and carbonation, Constr. Build. Mater. 112 (2016) 457–463.
[57] R. Talero, L. Trusilewicz, A. Delgado, C. Pedrajas, R. Lannegrand, V. Rahhal, R. Mejía, S. Delvasto, F.A. Ramírez, Comparative and semi-quantitative XRD analysis of Friedel's salt originating from pozzolan and Portland cement, Constr. Build. Mater. 25 (5) (2011) 2370–2380.
[58] H. Justnes, A review of chloride binding in cementitious systems, Nordic Concrete Research-Publications-, 1998, pp. 48–63.
[59] Q. Wang, G. Zhang, Y. Tong, C. Gu, Prediction on Permeability of Engineered Cementitious Composites, Crystals 11 (5) (2021) 526.
[60] E. Yang, Y. Yang, V.C. Li, Use of high volumes of fly ash to improve ECC mechanical properties and material greenness, ACI Mater. J. 104 (6) (2007) 620.
[61] A.K. Ammasi, Strength and durability of high volume fly ash in engineered cementitious composites, Mater. Today:. Proc. 5 (11) (2018) 24050–24058.
[62] M.D. Lepech, V.C. Li, Water permeability of cracked cementitious composites (2005).